Revisiting electron-correlation effects on valence shake-up satellites of neon

Noboru Watanabe and Masahiko Takahashi*
Institute of Multidisciplinary Research for Advanced Materials, Tohoku University, Sendai 980-8577, Japan

(Received 18 June 2019; published 20 September 2019)

We report an electron momentum spectroscopy study on valence shake-up satellites of neon. A symmetric noncoplanar (e, $2e$) experiment was performed at an incident electron energy of 1.2 keV, and the recoil-ion-momentum–dependent (e, $2e$) cross sections or momentum profiles of the shake-up satellites have been obtained. Furthermore, theoretical momentum profiles have been calculated on the basis of the distorted-wave Born approximation using configuration interaction wave functions of the initial neutral and final ionic states. Comparison between experiment and theory has revealed that contrary to a general expectation, electron correlation in the initial neutral state has a significant influence on the shapes of momentum profiles for neon satellites. It has been shown that the Dyson orbitals of transitions to the $2p^4(^1S)3s\,^2S$ and $2p^4(^1D)3p\,^2P$ ionic states are more localized than those of the associated primary ionizations due to electron-correlation effects.

DOI: 10.1103/PhysRevA.100.032710

I. INTRODUCTION

Two-hole–one-particle ($2h$-$1p$) excitations of atoms and molecules are of interest for investigating electron-correlation effects, since such multielectron processes cannot be described by the independent particle model. In the ionization spectra of atoms and molecules, $2h$-$1p$ excitations are represented by satellite lines, which fall at higher ionization energies than the main lines associated with single-hole ionic states [1,2]. In particular, when sufficiently high energy is transferred to the ejected electron, the $2h$-$1p$ states arise from a so-called shake-up mechanism in which a sudden change of potential due to the removal of an electron promotes another electron to an unoccupied orbital [2]. In this case, the satellite structure does not depend on second- and higher-order ionization mechanisms, such as two-step mechanisms [3,4], and is described by electron correlation in the target initial neutral and final ionic states. Shake-up satellites can thus provide a wealth of information about the many-electron wave functions of the target states and also offer a stringent test for many-body theories.

Simple atomic targets are especially suitable for the quantitative investigation of electron-correlation effects. The reason is that, in contrast to molecular targets, there is no influence of molecular vibration; the influence may appreciably affect the ionization cross sections [5,6], making it difficult to precisely extract electron-correlation effects on shake-up satellites. Besides, the interaction between the ejected electron and residual ion can be treated theoretically with high accuracy for atoms due to their single-center nature. Thereby, a number of studies on shake-up satellites have been performed for rare-gas atoms by means of high-energy photoelectron spectroscopy (PES) [2] and electron momentum spectroscopy (EMS) [7–15]. Nevertheless, there are still unresolved issues, even for a simple ten-electron atom, neon.

The first detailed EMS study of neon satellites was carried out by Brunger and Weigold in 1992 [8] and later extended by Samardzic *et al* [9]. In the studies, electron-impact ionization (e, $2e$) experiments were conducted, and the symmetries and spectroscopic factors of the valence satellite states were determined by means of the recoil-ion-momentum–dependent (e, $2e$) cross sections or momentum profiles. The data analysis was performed using the target Hartree-Fock approximation (THFA) [7], with general assumptions that electron correlation in the initial neutral state is not important and the satellite structure is governed by electron correlation in the final ionic states. Owing to the difficulty in measuring the weak satellite bands, there were inconsistencies between the EMS and PES results in certain details. To resolve this problem, we performed EMS measurements with improved statistical accuracy in 2005 [10]. The band assignments and values of the spectroscopic factors were thus revised, and the controversies in the earlier studies were largely resolved.

A remarkable exception is a satellite band at ionization energy of 55.83 eV; it exhibited an unexpected momentum profile whose shape could never be explained within the framework of the THFA. We therefore suggested the appreciable influence of electron correlation in the initial neutral state to this satellite band [10]. More recently, Li *et al.* [11] conducted high-energy-resolution EMS measurements on neon at an incident electron energy of 1.2 keV, together with theoretical calculations based on the plane-wave impulse approximation (PWIA) [7]. The symmetry-adapted-cluster configuration interaction (SAC-CI) wave functions [16–19] were used in the computation of momentum profiles to take into account electron correlation, not only in the final ionic states but also in the initial neutral state. The attempt [11], however, failed to reproduce the experimental result, and a significant discrepancy between experiment and theory has remained unresolved for the 55.83-eV band. Furthermore, most of the spectroscopic factors reported by Li *et al.* [11]

*Author to whom correspondence should be addressed: masahiko@tohoku.ac.jp

are considerably higher than those of our previous work [10], while the shapes of the momentum profiles obtained from the two studies [10,11] are properly in agreement. Clearly, further studies are needed to get a full understanding of neon satellites.

Under the circumstances, we have reinvestigated electron-correlation effects on the shake-up satellites of neon. In this work, an EMS experiment has been carried out for neon using an energy- and momentum-dispersive multichannel EMS spectrometer [20]. We have also performed theoretical calculations using configuration interaction (CI) wave functions. The distorted-wave Born approximation (DWBA) [7] has been applied to the calculations, since it is essentially important to take into account distortions of the incoming and outgoing electron waves (distorted-wave effects) [7] for properly describing $(e, 2e)$ processes in the inner-valence region with binding energies above ~30 eV. In such a high-binding-energy region, where many satellite bands appear, momentum profiles are appreciably influenced by the distorted-wave effects. For instance, it has been reported that neglecting the effects leads to significant overestimation of the inner-valence ionization cross sections of neon and hydrogen fluoride [10,21]. Despite the importance, however, theoretical calculations including both the initial-state correlation and distorted-wave effects, to our knowledge, have not been performed for shake-up satellites. By making comparisons between the experimental and theoretical results, the influences of electron correlation in the initial target state have been examined.

II. EXPERIMENT

EMS is a kinematically complete electron-impact ionization experiment under high-energy Bethe ridge conditions [7,22,23]. The ionization process of an atom A can be written as

$$e_0(E_0, \boldsymbol{p}_0) + A \rightarrow e_1(E_1, \boldsymbol{p}_1) + e_2(E_2, \boldsymbol{p}_2) + A^+,$$

where E_j's and p_j's $(j = 0, 1, 2)$ are the kinetic energies and momenta of the incident, inelastically scattered, and ejected electrons, respectively. Here A^+ denotes the residual ion. The binding energy E_{bind} and the recoil momentum of A^+, $\boldsymbol{q}$, can be determined by means of the energy and momentum conservation laws:

$$E_{\text{bind}} = E_0 - E_1 - E_2, \tag{1}$$

$$\boldsymbol{q} = \boldsymbol{p}_0 - \boldsymbol{p}_1 - \boldsymbol{p}_2. \tag{2}$$

The EMS experiment of neon was performed at $E_0 = 1.2$ keV in the symmetric noncoplanar geometry [7], where the scattered and ionized electrons having equal energies $(E_1 = E_2)$ and equal scattering polar angles of 45° are detected in coincidence. In the geometry, the magnitude of the recoil-ion momentum, $q = |\boldsymbol{q}|$, is related to the out-of-plane azimuthal angle difference between the two outgoing electrons $(\Delta\phi = \phi_2 - \phi_1 - \pi)$:

$$q = \sqrt{(p_0 - \sqrt{2}p_1)^2 + (\sqrt{2}p_1 \sin(\Delta\phi/2))^2}. \tag{3}$$

High-grade neon gas (Nippon Sanso, >99.999 95%) was used without further purification.

Details of the spectrometer used in the measurement are described elsewhere [20]. Briefly, it consists of an electron gun, a sample inlet system with eight gas nozzles, a spherical analyzer, and a pair of position-sensitive detectors. The electron gun produced an electron beam of typically 20 μA during the measurement. Experimental results were obtained by accumulating data at an ambient sample pressure of 3.0×10^{-4} Pa for ~ 4 weeks runtime. The resultant instrumental energy and momentum resolutions were 2.7 eV FWHM and about 0.19 a.u. at $q = 1.0$ a.u., respectively.

III. THEORETICAL CALCULATION

Within the distorted-wave Born approximation [7], the triple differential cross section (TDCS) of electron-impact ionization is given by

$$\frac{d^3\sigma}{dE_1 d\Omega_1 d\Omega_2} = (2\pi)^4 \frac{p_1 p_2}{p_0} \sum_{av} S_f \left| \left\langle \chi^{(-)}_{\boldsymbol{p}_1} \chi^{(-)}_{\boldsymbol{p}_2} \middle| V \middle| \varphi_f(\boldsymbol{r}) \chi^{(+)}_{\boldsymbol{p}_0} \right\rangle \right|^2, \tag{4}$$

with $\chi^{(+)}_{\boldsymbol{p}_0}$, $\chi^{(-)}_{\boldsymbol{p}_1}$, and $\chi^{(-)}_{\boldsymbol{p}_2}$ being distorted waves that describe the incoming and two outgoing electrons, respectively. Here V denotes the Coulomb potential and Σ_{av} represents a sum over all unresolved final ionic states. S_f and $\varphi_f(\boldsymbol{r})$ are the spectroscopic factor and the normalized Dyson orbital, which are defined by means of the overlap between the electronic wave functions of the N-electron initial neutral and $(N\text{-}1)$-electron final ionic states, ${\Psi_i}^N$ and ${\Psi_f}^{N-1}$:

$$\left\langle \boldsymbol{r} {\Psi_f}^{N-1} \middle| {\Psi_i}^N \right\rangle = \sqrt{S_f} \varphi_f(\boldsymbol{r}). \tag{5}$$

The q-dependent TDCS of a given ionization process is generally referred to as a momentum profile.

In EMS studies on satellites, the THFA has been widely used to analyze the data [8–10,12,13]. It assumes that the initial target state is adequately described by the Hartree-Fock (HF) wave function. Under the assumption, the normalized Dyson orbital $\varphi_f(\boldsymbol{r})$ of each ionization channel coincides with a canonical HF orbital, and it follows that the momentum profile of a satellite transition has almost the same shape as that of the associated primary ionization. Namely, within the THFA, the TDCS of a ^2S (^2P) satellite transition in neon exhibits a q dependence being quite similar to that of the $2s^{-1}$ ($2p^{-1}$) primary ionization [8–10], though there is a small discrepancy between them due to the difference of the ionization energies. Here the relative intensity of each satellite transition is governed by S_f, which corresponds to the probability of finding the $2s^{-1}$ ($2p^{-1}$) one-hole configuration in the final ionic state. Based on the above assumption, the values of S_f have been determined by comparing the intensity of each satellite band with that of the primary ionization or the THFA calculation [8–11].

In this work, we calculated theoretical momentum profiles without relying on the THFA to examine the influence of electron correlation in the initial neutral state. To this end, S_f and $\varphi_f(\boldsymbol{r})$ were obtained from the configuration interaction (CI) wave functions, which are expressed as superpositions of

TABLE I. Binding energies (eV) and spectroscopic factors ($10^2 \times S_f$) of neon.

	Expt [2].		CI Present work		QDPT-CI [27]		$4h$-$3p$ CI [28]		GF[a] [29]	
	E_{bind}	States	E_{bind}	S_f	E_{bind}	S_f	E_{bind}	S_f	E_{bind}	S_f
1	48.46	$2s^{-1}$	48.00	87.1	48.36	86.9	48.52	86.0	47.72	87.4
2	53.08	$2p^4(^3P)3p\,^2P$	52.88	0.38	52.94	0.39	52.61	0.44	54.05	0.29
3	55.83	$2p^4(^1S)3s\,^2S$	55.72	0.99	55.71	1.05	55.51	1.34	55.08	1.75
		$2p^4(^1D)3p\,^2P$	55.70	1.27	55.74	1.19	55.49	1.27	56.31	1.74
4	58.02	$2p^4(^3P)4p\,^2P$	58.01	0.37	57.89	0.27	57.64	0.35	58.21	0.004
5	59.49	$2p^4(^1D)3d\,^2S$	60.06	1.21	59.34	0.81	59.21	0.85	59.68	1.26
		$2p^4(^1S)3p\,^2P$	59.33	0.40	59.29	0.21	59.09	0.21	58.60	1.09

[a]Green's function (GF) calculation by Kheifets [29].

Slater determinants, Φ_s^N and Φ_t^{N-1}:

$$\Psi_i^N = \sum_s C_{is}^N \Phi_s^N, \tag{6}$$

$$\Psi_f^{N-1} = \sum_t C_{ft}^{N-1} \Phi_t^{N-1}, \tag{7}$$

where ${C_{is}}^N$ and ${C_{ft}}^{N-1}$ are coefficients of the CI expansions (CI coefficients). The theoretical wave functions were generated by means of the General Atomic Molecular Electronic Structure System (GAMESS) program [24]. In the calculations, atomic orbitals were constructed by means of the d-aug-cc-pVQZ Gaussian-type basis set [25,26] from which all g-type functions are excluded. For the initial neutral state, all singly and doubly excited configurations with respect to the single determinant ground state were taken into account, while the $1s$ orbital was kept doubly occupied. For the final ionic states, we calculated CI wave functions at the four-hole–three-particle ($4h-3p$) levels, which comprise all configurations with one, two, three, or four holes in the $2p$ and $2s$ valence orbitals and zero, one, two, or three electrons in the virtual orbitals.

Using the atomic orbitals $\psi_j(\boldsymbol{r})$, the normalized Dyson orbital can be written as

$$\varphi_f(\boldsymbol{r}) = S_f^{-1/2} \sum_j \langle \Psi_f^{N-1} | a_j | \Psi_i^N \rangle \psi_j(\boldsymbol{r}) \,, \tag{8}$$

with

$$S_f = \sum_j |\langle \Psi_f^{N-1} | a_j | \Psi_i^N \rangle|^2. \tag{9}$$

Here a_j denotes the electron annihilation operator for the jth orbital. From Eqs. (6) and (7), it follows that

$$\langle \Psi_f^{N-1} | a_j | \Psi_i^N \rangle = \sum_{s,t} \langle \Phi_t^{N-1} | a_j | \Phi_s^N \rangle C_{ft}^{N-1} C_{is}^N. \tag{10}$$

By means of Eqs. (8)–(10) the normalized Dyson orbitals and spectroscopic factors were calculated in this work. The theoretical binding energies and spectroscopic factors thus obtained are presented in Table I, together with other theoretical results reported in the literature [27–29].

Subsequently, the DWBA cross sections were calculated with the help of the computer program supplied from McCarthy [30]. Since McCarthy's program code was originally developed to make calculations of the TDCS with atomic orbitals expanded in Slater-type functions, we slightly modified it to be able to deal with Gaussian-type functions. To describe the incident and outgoing electrons, distorted waves were produced using the static potentials of the initial neutral and final ionic states, and the TDCSs were then calculated on the basis of Eq. (4).

As mentioned above, it has generally been assumed in EMS studies that the normalized Dyson orbital of a shake-up satellite is practically the same as that of the associated primary ionization, and on this basis, the spectroscopic factor has been determined from the intensity ratio between the momentum profiles of the satellite and the primary ionization [7–11]. This analysis procedure is applicable only when the influence of initial-state correlation is negligible. To examine the validity of the analysis procedure, additional calculations were performed for the satellites using the normalized Dyson orbitals of the $2p^{-1}$ and $2s^{-1}$ primary ionizations, as well as the theoretical spectroscopic factors of the satellites, calculations which are referred to as primary ionization calculations hereafter. All theoretical momentum profiles were folded with the instrumental momentum resolution (except otherwise noted) according to the procedure of Migdall *et al.* [31].

IV. RESULTS AND DISCUSSION

A. Binding energy spectra

Figure 1 presents a $\Delta\phi$-angle integrated binding energy spectrum of neon. It was constructed by plotting the number of coincidence events as a function of E_{bind}. Vertical bars indicate ionization energies taken from the photoelectron spectroscopy (PES) study [2]. Ionization bands are numbered according to the notation of earlier EMS studies on neon [9,10]. Band 1 corresponds to the $2s^{-1}$ primary ionization and bands 2–5 are attributed to $2h$-$1p$ excitations. The assignments of the bands are given in Table I.

In order to separate contributions of the individual ionization bands, a deconvolution procedure was used which assumes a Gaussian curve for each band. The center positions and widths of the Gaussian curves were inferred from the PES study [2] and the instrumental energy resolution, respectively, while the heights of the Gaussian curves were used as fitting parameters to reproduce the experimental result. The fitting procedure was applied to a series of binding energy spectra at each $\Delta\phi$, and the momentum profiles of the individual bands were subsequently constructed by plotting the area under the corresponding Gaussian curve against q.

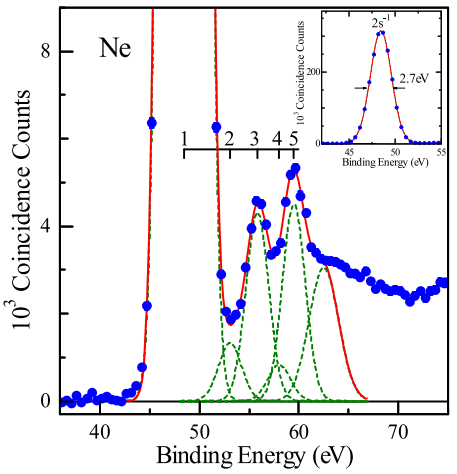

FIG. 1. Binding energy spectrum of neon. The dotted curves are the deconvolution functions and the solid curve is their sum. Vertical bars indicate ionization energies taken from the photoelectron spectroscopy study [2]. Inserted in the figure is the full view of the $2s^{-1}$ primary ionization band. The energy resolution has been inferred to be 2.7 eV from the FWHM of the $2s^{-1}$ peak.

B. Momentum profiles of the $2s^{-1}$ primary ionization

Figure 2 shows the experimental momentum profile of the $2s^{-1}$ primary ionization. Also depicted in the figure are two kinds of theoretical calculations. One is the THFA calculation and the other is the calculation with the CI wave functions, which are referred to as the HF momentum profile and the CI momentum profile, respectively, hereafter. For a comparison of the shapes, we normalized the experiment to the CI momentum profile so that the area in the region $q = 0.2$–2.0 a.u. was the same as that of the CI curve. In the same way, the HF curve was also scaled to the CI momentum profile by multiplying a factor of 1.05. The scaling factors thus obtained were subsequently applied to the results for the satellite bands. Hence, all experimental and theoretical momentum profiles share a common intensity scale. It can be seen from Fig. 1 that the CI momentum profile is in excellent agreement with experiment. Also seen from the figure is that although the HF momentum profile slightly underestimates the experiment at low q, the discrepancy is quite small, indicating a minor role of the initial-state electron correlation in the $2s^{-1}$ primary ionization.

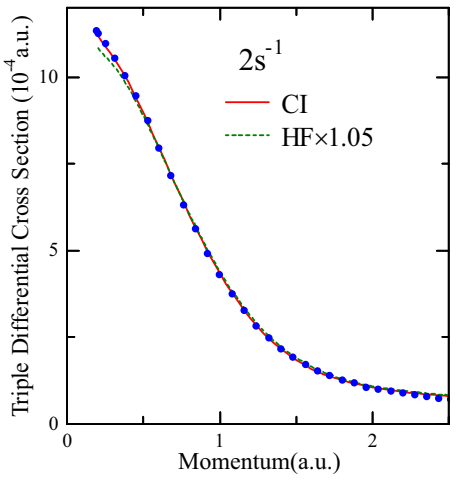

FIG. 2. Comparison between the experimental and theoretical momentum profiles of the $2s^{-1}$ primary ionization of neon. The solid and dashed lines represent the CI and HF momentum profiles, respectively, both of which are folded with the instrumental momentum resolution. The experimental and HF momentum profiles were, respectively, normalized to the CI momentum profile for a comparison of the shapes. See text for details.

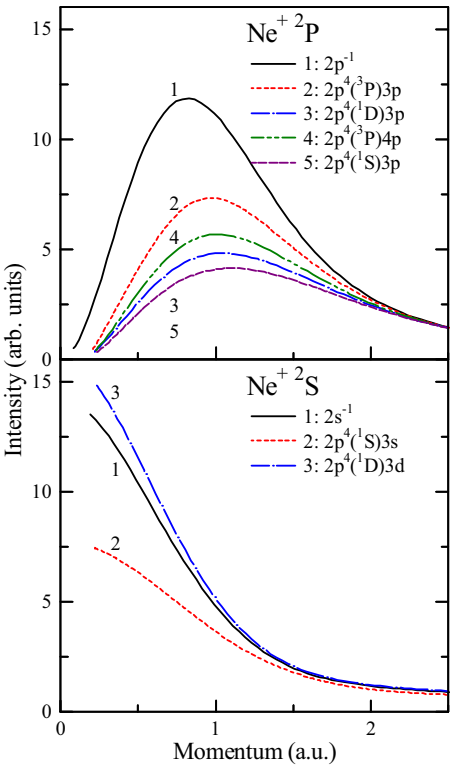

FIG. 3. The CI momentum profiles of the $2h$-$1p$ excitations as well as the primary ionizations. The upper panel presents the momentum profiles of the transitions to ^2P ionic states and the lower panel shows those of the transitions to ^2S ionic states. To facilitate comparison of the momentum-profile shapes, the values of the spectroscopic factors are all set to 1. The theoretical curves are not folded with the instrumental momentum resolution here.

C. Momentum profiles of satellite bands

We now turn our attention to the satellite transitions. Figure 3 shows the CI momentum profiles of the $2h$-$1p$ excitations, together with those of the $2p^{-1}$ and $2s^{-1}$ primary ionizations. The values of the spectroscopic factors are all set to 1 here to facilitate comparison of the momentum-profile shapes. The theoretical curves depicted are not folded with the instrumental momentum resolution, since no comparison with experiment is made in this figure. In general, a transition to a ^2P ionic state shows a "p-type" distribution, having a minimum at $q \sim 0$ a.u., while that to a ^2S ionic state has an "s-type" distribution with a maximum around the momentum origin. All the theoretical curves are in accord with this

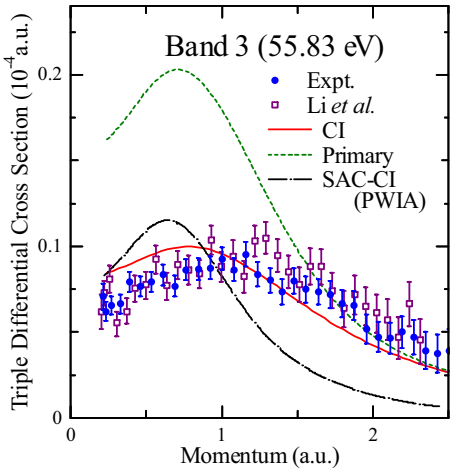

FIG. 4. Comparison between the experimental and theoretical momentum profiles of band 3 at 55.83 eV, which is composed of two unresolved satellites, one being the transition to the $2p^4(^1S)3s\,^2S$ ionic state and the other to the $2p^4(^1D)3p\,^2P$ ionic state. The solid line represents the CI calculation and the dashed line is the theoretical curve constructed from the momentum profiles of the $2s^{-1}$ and $2p^{-1}$ primary ionizations (primary ionization calculation). The theoretical momentum profiles are folded with the instrumental momentum resolution. Also depicted in the figure are the SAC-CI calculation [11], which is normalized to the CI curve at $q = 0.24$ a.u., and the experimental result reported by Li *et al.* [11] (open squares).

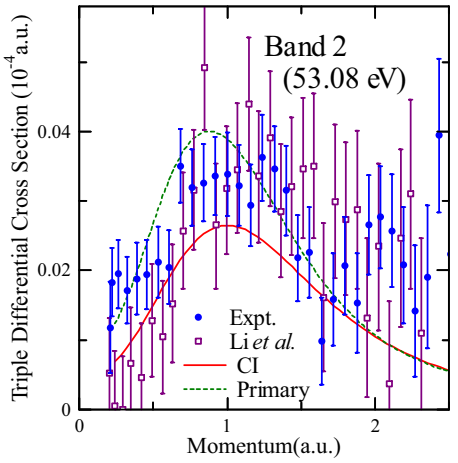

FIG. 5. Comparison between the experimental and theoretical momentum profiles of band 2 at 53.08 eV, which arises from transition to the $2p^4(^3P)3p\,^2P$ ionic state. The solid line represents the CI calculation, and the dashed line is the theoretical curve constructed from the momentum profiles of the $2s^{-1}$ and $2p^{-1}$ primary ionizations (primary ionization calculation). The theoretical momentum profiles are folded with the instrumental momentum resolution. For comparison, the experimental result reported by Li *et al.* [11] is also presented (open squares).

expectation, indicating that the symmetry of each satellite can easily be determined from the shape of the momentum profile.

A glance of Fig. 3 shows that the results for the ^2P satellite transitions are, though they all have p-type shapes, substantially different from the $2p^{-1}$ momentum profile. The peak positions shift towards higher q, and the maximum intensities are considerably lower than that of the primary ionization. The findings are contrary to general expectation, where the momentum profile of a satellite band has almost the same shape as that of the associated primary ionization, indicating the appreciable influence of electron correlation in the initial neutral state.

A notable deviation from the primary ionization has been observed also for the transition to the $2p^4(^1S)3s\,^2S$ ionic state. As can be seen from the lower panel of Fig. 3, the momentum profile of this transition has a much lower intensity than that of the $2s^{-1}$ primary ionization. On the other hand, the result of the $2p^4(^1D)3d$ ionization shows fair agreement with the $2s^{-1}$ momentum profile, as expected from the THFA. The CI calculation has revealed that the influence of initial-state electron correlation strongly depends upon the final ionic state of each satellite transition.

We subsequently compare the theoretical results with experiment. The momentum profiles of bands 2–5 are presented in Figs. 4–7. Also depicted in the figures are the experimental results reported by Li *et al.* [11]. Because their data have systematically higher intensities than ours, we have multiplied a factor of 0.65 to those for comparison in shape. The systematic intensity differences are unlikely to come from the uncertainty of our deconvolution procedure; if the error of the procedure leads to a decrease in intensity for some shake-up bands, the deconvoluted intensities of the other bands must become higher, since the total intensity is constant. The source of the inconsistency is not clear now, but it may be worthwhile to note that we have carefully determined the

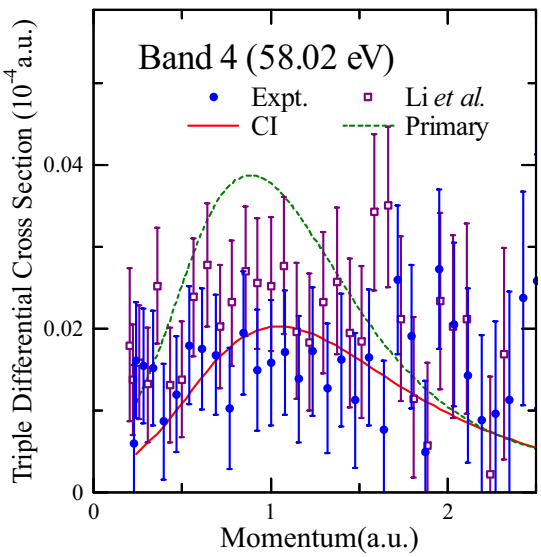

FIG. 6. Comparison between the experimental and theoretical momentum profiles of band 4 at 58.02 eV, which is ascribed to a transition to the $2p^4(^3P)4p\,^2P$ ionic state. The solid line represents the CI calculation, and the dashed line is the theoretical curve constructed from the momentum profiles of the $2s^{-1}$ and $2p^{-1}$ primary ionizations (primary ionization calculation). The theoretical momentum profiles are folded with the instrumental momentum resolution. For comparison, the experimental result reported by Li *et al.* [11] is also presented (open squares).

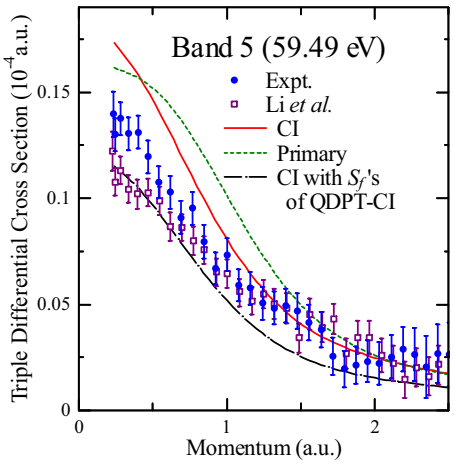

FIG. 7. Comparison between the experimental and theoretical momentum profiles of band 5 at 59.49 eV which stems from transitions to the $2p^4(^1D)3d\,^2S$ and $2p^4(^1S)3p\,^2P$ ionic states. The solid line represents the CI calculation, and the dashed line is the theoretical curve constructed from the momentum profiles of the $2s^{-1}$ and $2p^{-1}$ primary ionizations (primary ionization calculation). Also depicted in the figure is the CI momentum profile constructed by making use of the spectroscopic factors predicted by the QDPT-CI calculation [27] (chain line). The theoretical momentum profiles are folded with the instrumental momentum resolution. For comparison, the experimental result reported by Li *et al.* [11] is also presented (open squares).

relative intensities of the ionization bands and obtained results that are consistent with our previous work [10].

First, we focus on band 3 at 55.83 eV, for which the breakdown of the THFA has been suggested in our earlier study [10]. The band is composed of two unresolved satellites; one is the transition to the $2p^4(^1S)3s\,^2S$ ionic state and the other to the $2p^4(^1D)3p\,^2P$ state. It is evident from Fig. 4 that the primary ionization calculation significantly overestimates the experiment below $q \sim 1.5$ a.u., being consistent with our previous work and the high-resolution measurement by Li *et al.* On the other hand, the CI calculation has predicted much lower intensity at small q, and as a result, the deviation from the experiment is mostly resolved.

This is in sharp contrast to the theoretical result by Li *et al.* [11]. Their calculation on band 3, which is depicted in Fig. 4 for comparison, is in significant disagreement with experiment. There are two major differences between their calculation and ours. First, the SAC-CI approach was applied by Li *et al.* to the calculation of Dyson orbitals. Second, they computed the theoretical momentum profiles based on the plane-wave impulse approximation, while the DWBA was used in the present work. Concerning the latter difference, the incident and outgoing electrons are described by plane waves in the PWIA, assuming that the energies of the electrons are high enough to neglect the influence of the target potential. According to the PWIA, the $(e, 2e)$ cross section [7] is given by

$$\frac{d^3\sigma}{dE_1 d\Omega_1 d\Omega_2} = (2\pi)^4 \frac{p_1 p_2}{p_0} f_{\rm ee} \sum_{av} S_f |\varphi_f(\boldsymbol{q})|^2, \qquad (11)$$

where f_{ee} is the electron-electron collision factor and $\varphi_f(\boldsymbol{q})$ denotes the momentum-space representation of the normalized Dyson orbital. The PWIA thus directly relates the $(e, 2e)$ cross section to the momentum density distribution of the Dyson orbital, $|\varphi_f(\boldsymbol{q})|^2$. Although the PWIA has been widely used in EMS studies [7,22,23], distortions from the plane waves have been shown to be non-negligible for neon under the experimental conditions used [10,21]. The discrepancy between experiment and theory is thus due at least partly to the distorted-wave effect. However, its influence on the shapes of the momentum profiles is not significant [10] and cannot fully account for the huge deviation from the experiment.

The remaining possibility is the quality of the theoretical wave functions used. In the SAC-CI approach, unimportant unlinked terms have been neglected and a perturbation selection of the linked operators has also been performed to save computational costs [32]. Although these approximations have little influence on energy values, they may considerably affect the Dyson orbital of a satellite transition due to the following reason. The main configurations of the initial neutral and final ionic states are the HF configuration and a $2h$-$1p$ configuration, respectively. When constructing the Dyson orbital by means of Eqs. (8) and (10), the overlap between Slater determinants of the main configurations $\langle \Phi^{N-1}_{2h\text{-}1p} | a_j | \Phi^N_{\rm HF} \rangle$ vanishes owing to the orthogonality of the atomic orbitals and thus makes no contribution to the result. This implies that the Dyson orbitals of satellite transitions are not governed only by the main configurations. In other words, Slater determinants with small CI coefficients may have appreciable influence. Thereby, contributions from minor configurations should not be excluded in the calculation of Dyson orbitals, even if they are unimportant in energy calculations. By contrast to the SAC-CI calculation of Li *et al.*, the present work has taken into account all contributions from the constituent Slater determinants. This is the reason the CI prediction has shown much better agreement with experiment than the calculation by Li *et al.* The momentum profiles of shake-up satellites are highly sensitive to the small components of the target wave functions and can therefore provide a stringent test of the quality of the theoretical description of the electronic structure of the target.

Appreciable influences of the initial-state electron correlation have been recognized also for other satellite bands. Figures 5 and 6 show the momentum profiles of bands 2 and 4, which arise from transitions to the $2p^4(^3P)3p\,^2P$ and $2p^4(^3P)4p\,^2P$ satellite states, respectively. It can be seen from the figures that there are considerable differences between the CI and primary ionization calculations for both bands. Unfortunately, however, the data of band 2 have large error bars due to its low intensity as well as small separation in energy from the intense primary ionization; the large experimental uncertainties prevent us from a detailed assessment of the electron-correlation effects. On the other hand, the influence of initial-state electron correlation has exceeded the error bars for band 4; as can be seen from Fig. 6, the primary ionization calculation considerably overestimates the intensity at $q \sim 1.0$ a.u., while the CI momentum profile has been satisfactorily reproduced the experiment.

Figure 7 presents the experimental and theoretical momentum profiles of band 5 at 59.49 eV, which stems from

transitions to the $2p^4(^1D)3d\ ^2S$ and $2p^4(^1S)3p\ ^2P$ ionic states. Owing to the dominant contribution from the $2p^4(^1D)3d\ ^2S$ state, the experimental result shows an *s*-type shape. As mentioned above, the initial-state electron correlation gives only a small influence on the $2p^4(^1D)3d\ ^2S$ momentum profile. Hence, not only the CI momentum profile but also the primary ionization calculation is in fair agreement with experiment, though both calculations slightly overestimate the intensity at small q. The deviation is larger for the primary ionization calculation, due mainly to the influence of the initial-state electron correlation on the $2p^4(^1S)3p\ ^2P$ ionization. One may notice from Table I that for band 5, the present CI calculation predicts larger values of the spectroscopic factors than the other CI calculations, the quasidegenerate perturbation theory with CI (QDPT-CI) calculation by Fronzoni and Decleva *et al.* [27] and the $4h$-$3p$/$4h$-$4p$ CI calculation by Decleva *et al.* [28]. We thus constructed an additional CI momentum profile using the spectroscopic factors reported by Fronzoni *et al.* to infer the origin of the deviation from the experiment. The result is depicted as a chain line in Fig. 7. The experimental data lie between the two kinds of CI momentum profiles, indicating that the actual values of spectroscopic factors are between the two theoretical predictions used. It has been found that the experimental momentum profile can be well reproduced, if assuming spectroscopic factors of 0.0095 and 0.004 for the $2p^4(^1D)3d\ ^2S$ and $2p^4(^1S)3p\ ^2P$ satellite states, respectively.

D. Dyson orbitals

Within the PWIA, the $(e, 2e)$ cross section is proportional to the square modulus of the Dyson orbital in momentum space, which is related to the position-space representation by the Dirac-Fourier transform [see Eq. (11)]. Despite the distorted-wave effect being non-negligible, its influence on the shapes of momentum profiles is not significant for neon, and the present work may thus bring insights into the spatial distributions of the Dyson orbitals.

With this consideration in mind, we look into the momentum profile of band 3 again. As can be seen from Fig. 4, the experimental result is much broader than the primary ionization calculation. It strongly suggests that the associated Dyson orbitals have sharper distributions than those of the primary ionizations in position space, because the Fourier transform of a narrower function yields a broader function and vice versa. To confirm this, we subsequently compare the theoretical Dyson orbitals of the $2p^4(^1S)3s\ ^2S$ and $2p^4(^1D)3p\ ^2P$ satellite transitions with those of the $2p^{-1}$ and $2s^{-1}$ ionizations. The radial parts of the orbitals, $R(r)$'s, are shown in Fig. 8, which are multiplied by the distance from the nucleus, r. It can be seen from the figure that the Dyson orbital of the $2p^4(^1S)3s\ ^2S$ satellite transition is, as expected, more localized near the nucleus than that of the $2s^{-1}$ ionization due to the difference in electron-correlation effects. The same is true for the $2p^4(^1D)3p\ ^2P$ satellite transition.

It may be worthwhile to note that Dyson orbitals are not only related to the $(e, 2e)$ cross sections but are also required to calculate electronic factors of angular distributions of photoelectrons, Compton profiles, and are further relevant for other orbital imaging experiments [33]. Theoretical efforts have thus been devoted to the study of Dyson orbitals [33–35].

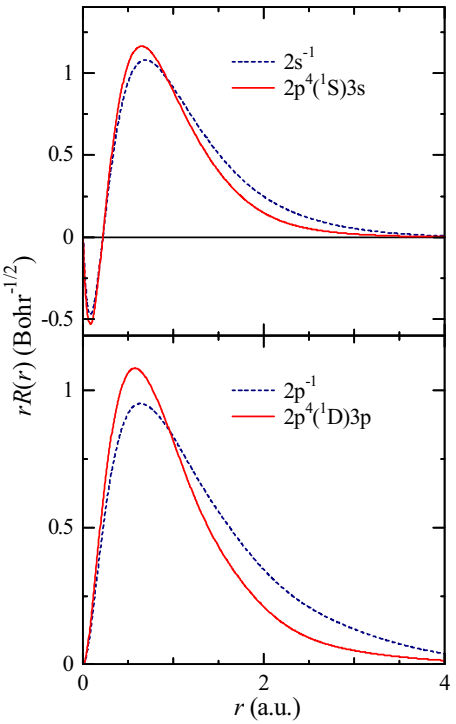

FIG. 8. Comparisons between the normalized Dyson orbitals of the primary ionizations and shake-up satellites. Shown in the figure are the radial parts of the orbitals multiplied by the distance from the nuclei, $rR(r)$'s. See text for details.

EMS can provide a powerful tool to experimentally investigate electron-correlation effects on Dyson orbitals.

V. SUMMARY

In this study, we have investigated electron-correlation effects on the $2h$-$1p$ excitations in neon. The momentum profiles of the shake-up satellites have been measured at an incident electron energy of 1.2 keV in the symmetric noncoplanar geometry. Theoretical momentum profiles have also been calculated using CI wave functions of the initial neutral and final ion states. Comparisons between experiment and theory have revealed that the initial-state electron correlation considerably affects the shapes of momentum profiles for the neon satellites, contrary to the expectation from the THFA. This implies that the spectroscopic factors cannot always be determined simply from the intensity ratio between each satellite and the primary ionization. For the 55.83-eV band, the inclusion of initial-state electron correlation has brought agreement with the experimental momentum profile and settled the controversy in the literature [10,11]. It has been shown that the momentum profiles of the shake-up satellites are highly sensitive to minor components of the target wave functions and can thus provide a stringent test of the quality of theoretical methods to describe the electronic structure of the target. Besides, it has been demonstrated that the momentum profiles provide information on the spatial distributions of the Dyson orbitals.

ACKNOWLEDGMENTS

This research was supported by the JSPS KAKENHI Grants No. 15H03761, No. 18H01932, and No. 25248002. It was also supported in part by the Management Expenses Grants for National Universities Corporation and the Cooperative Research Program of the Network Joint Research Center for Materials and Devices.

[1] T. A. Carlson, Phys. Rev. **156**, 142 (1967).
[2] S. Svensson, B. Eriksson, N. Mårtensson, G. Wendin, and U. Gelius, J. Electron Spectrosc. Relat. Phenom. **47**, 327 (1988), and references therein.
[3] R. J. Tweed, Z. Phys. D **23**, 309 (1992).
[4] N. Watanabe, M. Takahashi, Y. Udagawa, K. A. Kouzakov, and Yu. V. Popov, Phys. Rev. A **75**, 052701 (2007).
[5] N. Watanabe, M. Yamazaki, and M. Takahashi, J. Chem. Phys. **137**, 114301 (2012).
[6] N. Watanabe, M. Yamazaki, and M. Takahashi, J. Chem. Phys. **141**, 244314 (2014).
[7] I. E. McCarthy and E. Weigold, Rep. Prog. Phys. **54**, 789 (1991), and references therein.
[8] M. J. Brunger and E. Weigold, J. Phys. B: At. Mol. Opt. Phys. **25**, L481 (1992).
[9] O. Samardzic, S. W. Braidwood, E. Weigold, and M. J. Brunger, Phys. Rev. A **48**, 4390 (1993).
[10] N. Watanabe, Y. Khajuria, M. Takahashi, and Y. Udagawa, J. Electron Spectrosc. Relat. Phenom. **142**, 325 (2005).
[11] J. M. Li, Z. H. Luo, X. L. Chen, J. K. Deng, and C. G. Ning, Phys. Rev. A **92**, 032701 (2015).
[12] I. E. McCarthy, R. Pascual, P. Storer, and E. Weigold, Phys. Rev. A **40**, 3041 (1989).
[13] R. Nicholson, S. W. Braidwood, I. E. McCarthy, E. Weigold, and M. J. Brunger, Phys. Rev. A **53**, 4205 (1996).
[14] S. W. Braidwood, M. J. Brunger, and E. Weigold, Phys. Rev. A **47**, 2927 (1993).
[15] N. Watanabe, Y. Khajuria, M. Takahashi, Y. Udagawa, P. S. Vinitsky, Yu. V. Popov, O. Chuluunbaatar, and K. A. Kouzakov, Phys. Rev. A **72**, 032705 (2005).
[16] H. Nakatsuji, Chem. Phys. Lett. **59**, 362 (1978).
[17] H. Nakatsuji, Chem. Phys. Lett. **67**, 329 (1979).
[18] H. Nakatsuji, Chem. Phys. Lett. **67**, 334 (1979).
[19] H. Nakatsuji, Chem. Phys. **75**, 425 (1983).
[20] M. Takahashi, N. Watanabe, Y. Khajuria, K. Nakayama, Y. Udagawa, and J. H. D. Eland, J. Electron Spectrosc. Relat. Phenom. **141**, 83 (2004).
[21] S. W. Braidwood, M. J. Brunger, D. A. Konovalov, and E. Weigold, J. Phys. B: At. Mol. Opt. Phys. **26**, 1655 (1993).
[22] I. E. McCarthy and E. Weigold, Phys. Rep. **27**, 275 (1976).
[23] M. Takahashi, Bull. Chem. Soc. Jpn. **82**, 751 (2009).
[24] M. W. Schmidt, K. K. Baldridge, J. A. Boatz, S. T. Elbert, M. S. Gordon, J. H. Jensen, S. Koseki, N. Matsunaga, K. A. Nguyen, S. J. Su, T. L. Windus, M. Dupuis, and J. A. Montgomery, J. Comput. Chem. **14**, 1347 (1993).
[25] T. H. Dunning, Jr., J. Chem. Phys. **90**, 1007 (1989).
[26] D. E. Woon and T. H. Dunning, Jr., J. Chem. Phys. **100**, 2975 (1994).
[27] G. Fronzoni and P. Decleva, Chem. Phys. **220**, 15 (1997).
[28] P. Decleva, G. De Alti, G. Fronzoni, and A. Lisini, J. Phys. B: At. Mol. Opt. Phys. **23**, 3777 (1990).
[29] A. S. Kheifets, J. Phys. B: At. Mol. Opt. Phys. **28**, 3791 (1995).
[30] I. E. McCarthy, Aust. J. Phys. **48**, 1 (1995).
[31] J. N. Migdall, M. A. Coplan, D. S. Hench, J. H. Moore, J. A. Tossell, V. H. Smith Jr., and J. W. Liu, Chem. Phys. **57**, 141 (1981).
[32] M. Ehara, M. Ishida, K. Toyota, and H. Nakatsuji, *Reviews in Modern Quantum Chemistry*, edited by K. D. Sen (World Scientific, Singapore, 2002), pp. 293–319.
[33] C. M. Oana and A. I. Krylov, J. Chem. Phys. **127**, 234106 (2007).
[34] F. Morini, B. Hajgató, M. S. Deleuze, C. G. Ning, and J. K. Deng, J. Phys. Chem. A **112**, 9083 (2008).
[35] Y. R. Miao, C. G. Ning, and J. K. Deng, Phys. Rev. A **83**, 062706 (2011).